

Submitted to ApJ January 10, 1996

The Twisting X-ray Isophotes of the Elliptical Galaxy NGC 720

David A. Buote and Claude R. Canizares

Department of Physics and Center for Space Research 37-241,
 Massachusetts Institute of Technology
 77 Massachusetts Avenue, Cambridge, MA 02139,
 dbuote@space.mit.edu, crc@space.mit.edu

ABSTRACT

We present spatial analysis of the deep (57ks) ROSAT HRI X-ray image of the E4 galaxy NGC 720. The orientation of the HRI surface brightness is consistent with the optical position angle (*PA*) interior to semi-major axis $a \sim 60''$ (optical $R_e \sim 50''$). For larger a the isophotes twist and eventually ($a \gtrsim 100''$) orient along a direction consistent with the *PA* measured with the PSPC data (Buote & Canizares 1994) – the $\sim 30^\circ$ twist is significant at an estimated 99% confidence level. We argue that this twist is not the result of projected foreground and background sources, ram pressure effects, or tidal distortions. If spheroidal symmetry and a nearly isothermal hot gas are assumed, then the azimuthally averaged radial profile displays features which, when combined with the observed *PA* twist, are inconsistent with the simple assumptions that the X-ray emission is due either entirely to hot gas or to the combined emission from hot gas and discrete sources. We discuss possible origins of the *PA* twist and radial profile features (e.g., triaxiality).

1. Introduction

The intrinsic shapes of elliptical galaxies are currently not well understood (e.g., de Zeeuw & Franx 1991; de Zeeuw 1995). Hydrodynamic simulations of galaxy halos in a Cold Dark Matter universe typically produce flattened ($\epsilon \sim 0.5$), oblate-triaxial halos (e.g., Katz & Gunn 1991; Dubinski 1994). Yet there is a paucity of observational constraints for the intrinsic shapes and, in particular, the degree of triaxiality in ellipticals. For a handful of galaxies the intrinsic shapes have been precisely measured and suggest highly elongated halos with $\epsilon \sim 0.6$ (e.g., Sackett 1995), though the degree of triaxiality has not been constrained. Recently, Statler (1994a,b) has shown that in principle the stellar velocity fields can effectively probe triaxiality of ellipticals, however the observations required are extensive and the current constraints allow for a large range of triaxial shapes.

The E4 galaxy NGC 720 is a promising candidate for analysis of the shapes of its X-ray isophotes because it should not be substantially affected by ram pressure or tidal distortions

due to it being very isolated from other large galaxies (Schechter 1987). Moreover, NGC 720 is quite bright in the ROSAT band (8×10^{-13} erg cm $^{-2}$ s $^{-1}$ for 0.5–2.0 keV) and is likely to be dominated by emission from hot gas as indicated by its large ratio of X-ray to optical luminosity (Kim, Fabbiano, & Trinchieri 1992). Also, radio emission has not been detected from NGC 720 (e.g., Birkinshaw & Davies 1985) indicating that the gas should not be substantially disturbed by magnetic fields. Since environmental effects should be unimportant, the X-ray emissivity should trace the shape of the three-dimensional gravitational potential, independent of the temperature profile of the gas (Buote & Canizares 1994, 1996); though possible rotation of the hot gas may affect the emissivity shape in the core (see §5). Thus, the X-ray isophote shapes and orientations probe the intrinsic shape of the potential, and hence the mass, of the galaxy.

From analysis of ROSAT Position Sensitive Proportional Counter (PSPC) data of the E4 galaxy NGC 720 Buote & Canizares (1994, hereafter BC) concluded that the isophote shapes and radial profile of the X-ray emission requires an extended, massive, flattened dark halo ($\epsilon \sim 0.5 - 0.7$). However, the X-ray isophotes at $a \sim 100''$ are misaligned by $\sim 30^\circ$ from the optical isophotes, a fact that was not incorporated into the analysis of BC. The orientations of the inner X-ray isophotes ($a \lesssim 60''$) are not well determined by the PSPC data because of the width of the point spread function (PSF) ($\sim 30''$ FWHM). To better understand the nature of this measured misalignment between X-ray and optical isophotes, we obtained a high resolution observation to specifically address the orientation of the X-ray contours at small radii.

2. Observations and Data Analysis

From January 8–12, 1994 NGC 720 was observed with the High Resolution Imager (HRI) on board ROSAT (Trümper 1983) resulting in an effective exposure of 57ks; for descriptions of the ROSAT X-ray telescope see Aschenbach (1988) and the HRI see David et al. (1995). The spatial resolution of the HRI is $\sim 4''$ FWHM, but the HRI possesses only limited spectral resolution in its 0.1 – 2.4 keV pass-band.

To prepare the HRI image for spatial analysis we (1) rebinned the image into a more manageable 1638×1638 field of $2.5''$ pixels, (2) searched for time intervals where the background was anomalously high, (3) flattened the image, (4) selected PHA channels 1–5 to optimize signal-to-noise ratio (S/N), (5) examined the accuracy of the aspect solution, (6) removed foreground and background sources embedded in the galactic continuum, and (7) subtracted the background. All of the reduction procedures were implemented with the standard IRAF-PROS and FTOOLS software.

By masking out detected sources in the HRI field (including NGC 720 itself using a circle of $10'$ radius), we constructed the background light curve which shows no significant fluctuations above those expected for the HRI due to external radiation (David et al. 1995). The image was flattened with the exposure map generated by the task *hriexpmap* in FTOOLS; note that the true

resolution of this exposure map actually corresponds to $5''$ pixels. The ground calibration results of David et al. (1995) show that several PHA channels have low S/N . We examined the effects of the PHA channels on S/N for a circle of $50''$ radius centered on NGC 720; the background was taken from an annulus centered on NGC 720 with ($r \sim 7'$, $\Delta r = 1'$) with sources masked out. Including only PHA channels 1-5 optimized the S/N which is consistent with the results of David et al., with the possible exception of channel 1 for which David et al. concluded also has low S/N .

Since we are concerned in this paper with measurements of position angles and ellipticities of the X-ray isophotes in NGC 720 an accurate aspect solution for the HRI observation is essential. The point sources in the field are not sufficiently bright to usefully perform the aspect correction algorithm proposed by Morse (1994). Hence, we examined the aspect solution individually for the different observational intervals (OBIs); i.e. those time intervals where the spacecraft continuously pointed on NGC 720. From analysis of the point sources in the fields of the three OBIs with appreciable exposures we find no statistically significant relative shifts of the OBIs. Typically, the required shifts were 0.4 ± 0.8 pixels (i.e. $1'' \pm 2''$). The effects of the small shifts consistent with this result are insignificant when considering the measurement of ellipticities and position angles on scales of interest to this study (i.e. $\gtrsim 15''$).

There is one point source $150''$ to the SE, another $200''$ to the NW, and 4 more straddling the circle of $400''$ radius from the galaxy; within $\sim 2'$ of the center of NGC 720 there are no obvious point sources. Since we cannot obtain useful constraints on the ellipticity and position angle of the X-ray isophotes for $r > 100''$ due to inadequate S/N we simply remove these sources. We removed sources by first choosing an annulus around each source to estimate the local background. We then fitted a second order polynomial surface to the background and replaced the source with the background. This procedure is well suited for estimating quadrupole moments of high S/N cluster images; see Buote & Tsai (1996) for a thorough discussion. The effects of unresolved points sources on the shapes and orientations of the isophotes are examined in the next section.

The reduced image is plotted in Figure 1, where for display we have rebinned the image into $5''$ pixels and smoothed with a Gaussian of $\sigma = 1$ pixel.

The final step in the image reduction is to subtract the background. We only require background subtraction for computation of the radial profile, not for computation of the ellipticities and position angles. Since we extend the radial profile into regions where the galaxy flux \lesssim background level we need to carefully estimate the background to reduce large fractional systematic errors in the radial profile at large radii. The HRI surface brightness profile of NGC 720 reaches the background level for $r \sim 300''$, somewhat smaller than the outer radius $r \sim 400''$ we detected with the more sensitive PSPC (BC).

To estimate the background level we compared circular annuli of different radii centered on NGC 720. We restricted analysis to regions outside of $r = 400''$ to minimize residual contribution from the galaxy. Moreover, to reduce any errors in the HRI vignetting correction and possible scattered light in the outer regions of the HRI image we confined our analysis to regions as near

the center of the field as possible. From consideration of these issues we adopted the $500'' - 600''$ annulus to estimate the background level where the residual contribution to the emission from NGC 720 should be $< 1\%$. We estimate that this background level is accurate to within $\sim 3\%$.

3. X-ray Isophote Shapes and Orientations

As is typical for X-ray images of early-type galaxies the small number of counts (~ 1000) for the HRI image of NGC 720 implies that we can only hope to measure with any precision the ellipticity and position angle of the aggregate X-ray surface brightness in a large aperture. The method we employ is an iterative procedure and is analogous to computing the two-dimensional moments of inertia within an elliptical region where the ellipticity, ϵ_M , is given by the square root of the ratio of principal moments and the orientation of the principal moments gives the position angle, θ_M (see BC; Buote & Canizares 1996). The parameters ϵ_M and θ_M are good estimates of the ellipticity (ϵ) and position angle (θ , or PA) of an intrinsic elliptical distribution of constant shape and orientation. For a more complex distribution ϵ_M and θ_M are average values weighted heavily by the outer parts of the regions.

To estimate the uncertainties on ϵ_M and θ_M we employ a Monte Carlo procedure described by Buote & Tsai (1996) slightly modified for application to HRI images. Because the HRI surface brightness profile of NGC 720 appears to be rather complex in shape and orientation, we apply the Monte Carlo procedure directly to the HRI image rather than some best-guess model (e.g., an elliptical β model) which may not account for all of the relevant features. To construct an “average” model for the real HRI image we smooth the reduced image (including background) with a Gaussian of width $\sigma = 2.5''$ (approximately half the width of the on-axis HRI PSF) to better approximate pixels with 0 counts in the real image. We examined the sensitivity of the derived values of ϵ_M and θ_M to the value of σ . The estimated 68% confidence limits on ϵ_M and θ_M for semi-major axes $\gtrsim 30''$ typically vary by $< 10\%$ for values of $\sigma = 0'' - 2.5''$. For $\sigma = 5''$ the derived confidence estimates for these semi-major axes vary by as much as 25%. However, for semi-major axes $\gtrsim 75''$ the 68% confidence limits vary by $< 5\%$ for $\sigma = 0'' - 5''$.

To the smoothed image we added point sources having spatial properties consistent with the HRI PSF and numbers consistent with the $\log N(> S) - \log S$ distribution given by Hasinger et al. (1993). We excluded from the simulations any bright point sources (i.e. $> 5\sigma$ above the background) appearing within $\sim 100''$ of the galaxy center as they would be easily detected by visual examination and removed. Poisson noise was then added to the image consistent with the exposure of the NGC 720 HRI observation.

We performed 1000 realizations and defined the 90% (for example) confidence limits on ϵ_M and θ_M for each semi-major axis to be the 50th smallest and the 50th largest values obtained from the 1000 simulations. Although this definition is arbitrary it provides a simple, realistic measure of the significance of the ellipticity and PA.

In Table 1 we list the results for ϵ_M and θ_M and their associated 68% and 90% confidence estimates for semi-major axes (a) ranging from $10''$ to $120''$. The isophotes are significantly elongated with $\epsilon_M \sim 0.3 \pm 0.1$ for $10'' \leq a \leq 120''$. These values for ϵ_M are consistent with the PSPC values (BC) for $a \gtrsim 75''$ but are systematically larger than those obtained with the PSPC for $a \lesssim 75''$, which is consistent with the PSPC values at small a being reduced as a result of its larger PSF.

The position angles of the isophotes vary significantly with semi-major axis; the PA profile and the estimated 2σ errors are plotted in Figure 2. For $a \lesssim 60''$, the PA is consistent with the optical PA of 142° (e.g., Peletier et al. 1990). At larger a , however, the PA decreases and levels off at values consistent with $PA = 114^\circ$, the position angle obtained from analysis of the PSPC at these a . The variation is highly significant: for $a = 90''$ we estimate that $PA = 99^\circ - 132^\circ$ at the 95% confidence level, and $PA = 90^\circ - 137^\circ$ at the 99% level, still significantly less than the measured value of 144° at $a = 60''$.

Possible origins for this PA twist are chance alignments of a few appropriately placed unresolved foreground and background sources, the residual effects of ram pressure distortions, or tidal interactions with neighboring galaxies. For the case of tidal fields, there are no giant galaxies within 1 Mpc [Dressler, Schechter, & Rose 1986] which means that the expected gravitational field due to a neighbor comparable in size to NGC 720 would contribute only 1% to the potential at a radius of 10 kpc from NGC 720. If the other effects are important then the surface brightness should display substantial departures from elliptical symmetry. To investigate this possibility we first examined whether the centroid of the surface brightness shifts with increasing aperture size. Over the whole range of a explored the centroid shifts by less than one pixel in both x and y directions; i.e. there is no significant centroid shift.

We also examined higher order symmetry. First, we aligned coordinate axes centered on the galaxy with the x axis at the optical $PA = 142^\circ$. Within a radius of $r = 60''$ we computed the counts in the four quadrants in these coordinates. The results are listed in Table 2. The counts are consistent with a mean value of ~ 285 and their 1σ Poisson uncertainties of 22; i.e. within $r = 60''$ there is no evidence for asymmetry between the four quadrants. By instead aligning the coordinate axes with $PA = 114^\circ$ and examining the surface brightness in an annulus from $r = 60'' - 90''$ we explored the symmetry in the outer regions; see Table 2. Again, there is no evidence for asymmetries.

Unresolved point sources (and statistical noise) cannot produce the observed PA twist as demonstrated by the above Monte Carlo simulations (Table 1). To further investigate this issue we estimated the probability that unresolved sources contribute sufficiently to (specifically) the outer, low surface brightness, isophotes to produce the position angle twist. The region of interest lies between the isophotes with $a \sim 75'' - 100''$. If part of this region is significantly contaminated by point-source emission, then a PA twist could result. Consider, e.g., a $25'' \times 25''$ square within this region in which the flux from NGC 720 is measured to be $\sim 4 \times 10^{-15}$ erg cm $^{-2}$ s $^{-1}$ in the

0.1-2.4 keV band using the PSPC image. From the $\log N(> S) - \log S$ distribution for ROSAT X-ray sources (Hasinger et al. 1993) we estimate the probability that there is a source with flux at least half of the measured value in the square region to be only $\sim 2\%$. Hence, it is unlikely that the gross features of the surface brightness in the key regions $r \sim 75'' - 100''$ are affected substantially by the emission from unresolved foreground and background sources.

4. Radial Profile

Using the background-subtracted HRI image we constructed the azimuthally averaged radial profile located at the centroid of the galaxy emission. The centroid was computed in a circular aperture of radius $120''$ which effectively encloses $\sim 85\%$ of the total flux of the galaxy; note that the centroid varies by $< 2.5''$ for smaller aperture sizes. The radial profile was rebinned so that each bin had $S/N \geq 6$. This yields six $5''$ bins from $r = 0'' - 30''$, three $15''$ bins from $r = 30'' - 75''$, and one $45''$ bin from $r = 75'' - 120''$. The radial profile is plotted in Figure 3.

For $r \gtrsim 30''$, the radial profile is consistent with a power-law form. However, the profile appears to level off between $r \sim 10'' - 30''$ and then rises again for $r \lesssim 10''$. These qualitative features of the radial profile appear to be robust to small changes in the sizes of the radial bins. As we show in the next section, although these features are not of sufficient S/N to distinguish between a wide range of models, they are of sufficient quality to eliminate some of the simplest models that previously were consistent with the X-ray data for NGC 720.

5. Analysis and Discussion

Since the emission from unresolved foreground and background sources and effects from ram pressure and tidal distortions appear to be insignificant (see §3), we now consider origins of the surface brightness features that are intrinsic to the galaxy. First we examine whether the HRI data may be described by a model where the X-ray emission is entirely due to hot gas in hydrostatic equilibrium with the underlying potential of NGC 720. We shall consider two classes of models – β models and power-law or Hernquist Spheroidal Mass Distributions (SMDs). First we take the surface brightness distribution to be given by the β model (Cavaliere & Fusco-Femiano 1976), $\Sigma_{hg}(R) = \Sigma_0 [1 + (R/R_c)^2]^{-3\beta+1/2}$, which is a power law for $R \gg R_c$. This model corresponds to a logarithmic potential at large radii (e.g., Appendix C. of Trinchieri et al. 1986) and is generally a good fit to the X-ray radial profiles of ellipticals observed with the *Einstein* IPC (e.g., Forman, Jones, & Tucker 1985; Trinchieri et al. 1986) and the ROSAT PSPC – in particular that of NGC 720 (see BC).

To perform a more consistent comparison between the model and data we evaluate the model on a grid of pixels corresponding to the same scale as the data and convolve the model with the relevant PSF. The radial profile is then constructed and binned in the same manner as done for

the data. This procedure does yield slightly different parameter values and χ^2 values than if the convolved model is directly compared to the radial profile of the data as is typically done. In all of the fits we set the ellipticity of the hot gas to $\epsilon_x = 0.25$ which is essentially the mean value of the X-ray isophotes. The fitted parameters and χ^2 values change by $\lesssim 5\%$ when considering ellipticities $\epsilon_x = 0.2 - 0.3$.

The β model is a poor fit to the HRI radial profile: $\chi^2 = 18$ for 7 dof. The poor quality of the fit is due entirely to the inner radial bins ($r \leq 30''$). In contrast, BC showed that the β model provides a good fit to the PSPC profile of NGC 720. We reanalyzed the PSPC data and rebinned the PSPC radial profile so that each bin has $S/N > 5$ and energy range 0.5-2.0 keV; BC instead fixed the bin size to $15''$. The β model applied to this rebinned PSPC radial profile yields a formally marginal fit: $\chi^2 = 19$ for 10 dof. Similar to the HRI data, the major source of discrepancy between model and data is due to the two inner bins ($0'' - 15'', 15'' - 30''$) – the bin near $90''$ is not as important due to its larger fractional statistical uncertainty. The best-fit parameters for the HRI and PSPC fits are listed in Table 3. The HRI profile is shallower (i.e. smaller β) than that of the PSPC which is probably an artifact of the weak constraints at large radii ($r \gtrsim 100''$); i.e. when the PSPC data is fit only to bins within $r = 100''$ then smaller β values are also obtained.

It is necessary to fit the model jointly to the HRI and PSPC data in order to obtain constraints acceptable for both data sets; the model for each data set is convolved with its appropriate PSF. By doing this we now have four free parameters: a_x , β , and the normalizations for the HRI and PSPC radial profiles. The joint fit is shown in Figure 3 and the best-fit and 90% confidence levels (2 interesting parameters) are shown in Table 3. The fit is formally worse ($\chi^2 = 53$ for 19 dof) than the fits to the data sets individually which is primarily due to joining the shallower HRI profile to the steeper PSPC profile; note the poor fit is not the result of the small (< few %) uncertainties in the background estimates.

These qualitative and quantitative results are reproduced when we consider the spheroidal mass models (SMDs) used in BC that are consistent with the PSPC spatial and spectral (i.e. nearly isothermal) data; i.e. models where the mass density is stratified on concentric, similar spheroids and has either a power-law or Hernquist (1990) radial profile. For example, a model with mass density $\rho \sim r^{-2}$ and an ellipticity of 0.50 fit jointly to the HRI and PSPC data yields a poor fit: $\chi^2 = 46$ for 19 dof. Similar results are obtained for Hernquist (1990) models and its generalization to shallower profiles (i.e. $\rho \sim r^{-1}(a_c + r)^{-1}$). Hence, simple plausible models for the hot gas cannot fit the radial profiles of the HRI and PSPC data, where the disagreement between models and data primarily occurs in the inner regions $r \lesssim 30''$.

We are thus compelled to increase the complexity of our model to fit the X-ray surface brightness. There must be significant contribution to the X-ray emission from discrete sources in NGC 720; i.e., the integrated emission from X-ray binaries (see, e.g., Canizares, Fabbiano, & Trinchieri 1987; Kim, Fabbiano, & Trinchieri 1992). This “discrete” component should have a spectrum that is harder than that of the hot gas and essentially similar to that found in spirals

where discrete sources are likely to account for most of the emission.

Considering the relatively large value of L_X/L_B for NGC 720 we do not expect a large contribution to the X-ray emission from discrete sources in the 0.1 - 2.4 keV energy range (Kim et al. 1992). We estimate the relative flux of the hot gas and a harder component using the PSPC spectrum computed in a circle of 120'' about the galaxy centroid. We fitted the spectrum with two Raymond-Smith (1977, updated to current version) models where we fixed the column density to its Galactic value (Stark et al. 1992), the abundances to 20% solar (approximately the best-fit single-component value – see BC), and the temperature of the hard component to 4.5 keV which corresponds to the integrated spectrum of Sb+Sc galaxies analyzed by Kim et al. (1992). This temperature is also consistent with the hard component determined for NGC 4472 with ASCA (Matsushita et al. 1995), a galaxy that has a value of L_X/L_B very similar to NGC 720. We find for these models that the emission of the hard component can make up at most 32% of the total emission within 120'' (90% confidence on two interesting parameters) but with a lower limit approaching zero (0.1%). This range is consistent with the ASCA observation of NGC 4472 where Matsushita et al. (1995) determined that only $\sim 16\%$ of the X-ray emission in the 0.5 - 5 keV band is due to a hard component (for about twice the radius used for NGC 720). In the 0.1-2.4 keV band of the HRI and PSPC this percentage should be even smaller.

We place alternative constraints on the total emission from discrete sources using the spatial properties of the X-ray surface brightness. Although there exists no strong observational constraints on the spatial distribution of such a component in ellipticals, we make the reasonable assumption that the discrete emission has a spatial distribution similar to that of the optical light. We take the surface brightness of the discrete component, Σ_{ds} , to have the two-dimensional distribution of the B -band light of NGC 720: the HST data from Kormendy et al. (1993) define the core while the rest of the galaxy is defined by the data from Peletier et al. (1990), who find no evidence for color gradients in NGC 720. The hot-gas component, Σ_{hg} , is again modeled as either the β or the isothermal power-law or Hernquist (1990) SMDs.

In order to specify the parameters of this discrete + hot gas model we fitted this model jointly to radial profiles of the HRI and PSPC data, convolved with the appropriate PSFs, and using the same procedure as above. The HRI data provide the dominant constraint at small radii ($R \lesssim 30''$) while the PSPC data dominates over the rest of the galaxy ($R \sim 30'' - 400''$). For each fit the ratio of emission from hot gas to the emission from discrete sources, Σ_{hg}/Σ_{ds} , is computed in a circle of radius 120'' from the galaxy centroid.

The results of the joint fits to the HRI and PSPC radial profiles are listed in Table 3 and shown in Figure 3. Let us first consider the case where the hot gas is taken to be a β model. The range of ratios of discrete emission to hot gas obtained are consistent with the above spectral results from the PSPC which serves as a comforting consistency check between the spatial and spectral methods. Although only one free parameter has been added (Σ_{hg}/Σ_{ds}) to our model, the quality of the fit is substantially improved ($\chi^2 = 29$ for 18 dof), though still formally only

a marginal fit ($P_{\chi^2} = 95\%$). Again the discrepancy between model and data may be attributed primarily to the inner $30''$ region. The model fits the PSPC profile acceptably, but the HRI profile (particularly the core) is poorly fit: $\chi^2_{PSPC} = 13$ for 9 dof and $\chi^2_{HRI} = 15$ for 6 dof. In contrast to the hot gas alone, adding the discrete component allows the innermost bin to be well fitted (i.e. this combined hot gas + discrete model can account well for the excess emission in the central bin). However, this model does not produce the flattening of the HRI radial profile between $r \sim 10'' - 30''$, which is the dominant source of discrepancy between model and data. When the hot gas is modeled using the SMDs (see above) we obtain results in excellent agreement with the β models (see Table 3).

Although the formal fit to the data is marginal, it is worth examining whether the discrete + hot gas model can reproduce the observed position angle twist. We take the discrete model to be oriented along the optical PA while the hot gas is oriented along the PA of the outer isophotes ($PA = 114^\circ$). We find that the models do not produce large PA twists, the largest twist is generally produced by the best-fit model to the radial profile where $\Delta PA \sim 10^\circ$ between semi-major axes of $60''$ and $100''$. The statistical uncertainties on simulated observations of these models are rather large and similar to what was found for the data (Table 1): the observed PA twist between semi-major axes of $60''$ and $100''$ is inconsistent at the estimated $\sim 90\%$ confidence level. Since, however, an acceptable model must produce the *PA profile* between $60''$ and $100''$ (not simply the endpoints), the discrepancy may be more pronounced. (This issue requires significantly more computational effort to properly address than is appropriate for our present study.) Hence, the discrete + hot gas model cannot fully produce the observed large PA twist (though it will contribute) or the features in the core of the radial profile.

Joint consideration of the HRI and PSPC data of NGC 720 suggests that the X-ray emission is more complex than simple isothermal spheroidal models of the hot gas combined with emission from discrete sources. Detailed investigation of more sophisticated models is beyond the scope of this paper, but we briefly describe some possible solutions.

Triaxiality: A PA twist can be produced by the projection of a triaxial distribution whose three-dimensional isodensity surfaces have shapes which vary as a function of radius (e.g., Mihalas & Binney 1981). The ellipticities of the optical isophotes do not vary substantially over the region of interest ($a \gtrsim 30''$; e.g., Peletier et al. 1990). However, the stars do not trace the same shape as the potential (because of anisotropic velocity dispersions) and thus do not in general have the same three-dimensional spatial distribution, and thus projected distribution, as the gas. N-body simulations of galaxies and clusters generically produce strongly triaxial halos (e.g., Frenk et al. 1988; Dubinski & Carlberg 1991). In fact, hydrodynamic simulations often produce halos that are nearly oblate in the central regions while the outer parts, particularly for clusters formed in filaments, are nearly prolate (e.g., Katz & Gunn 1992; Dubinski 1994; Buote & Tsai 1995). Perhaps a large observed PA twist can result if the transition from oblate ($r \lesssim 60''$) to prolate ($r \gtrsim 100''$) is sufficiently rapid. However, using simple models with the above specifications and a power-law variation in axial ratio between $a \sim 60''$ and $a \sim 100''$ we find it difficult to produce

PA twists larger than $\sim 15 - 20^\circ$ which also produce the observed ellipticities of the isophotes.

Intrinsic Misalignment of Light and DM Halo: If the principal axes of the stars and dark matter halo are intrinsically misaligned then a *PA* twist would naturally occur. Such a scenario has been proposed by Ostriker & Binney (1989) to explain the origin of warps in disk galaxies. However, Dubinski & Kuijken (1995) have shown that large misalignments will rapidly decay because the disk, with its large spin misaligned with the halo, will precess and suffer dynamical friction with the halo, and thus settle into the halo equatorial plane; often the inner halo actually aligns with the disk because the disk is difficult to re-orient due to its large spin. Because a giant elliptical like NGC 720 does not rotate substantially ($v/\sigma^* = 0.15$, e.g., Fried & Illingworth 1994), it is not clear whether these arguments imply the same short timescales. Perhaps another mechanism (e.g., phase mixing) ensures alignment for an elliptical. Even if the timescale for alignment is found to be short compared to a Hubble time (thus ruling out a primordial misalignment), it may be that the misalignment is caused by a dwarf companion that has recently struck NGC 720; there are several known dwarf companion galaxies around NGC 720 (Dressler et. al. 1986).

Rotating Cooling Flow: The flattening of the radial profile between $r \sim 10'' - 30''$, though not of high enough significance to warrant detailed modeling, deserves some attention. It is possible that the surface brightness features on these small scales are due to patchy absorption by cold clouds condensed out of the hot phase (e.g., Fabian 1994). However, another aspect of the cooling gas may be the origin for the features. Even though giant ellipticals like NGC 720 typically rotate slowly, in principle slowly rotating gas at large galacto-centric radii can cool, flow towards the center, eventually be driven to dynamically important rotational velocities if angular momentum is conserved (e.g., Cowie, Fabian, & Nulsen 1980), and thereby form a spinning disk (e.g., Kley & Mathews 1995). Not only will the ellipticity of the X-ray isophotes become more elongated in the region of dynamically important rotation, the shape of the radial profile will be affected as well (e.g., Kley & Mathews 1995).

6. Conclusions

The interesting features of the HRI surface brightness of NGC 720 provide more questions than answers into the origin of its X-ray emission and the distribution of its underlying mass. Presently ASCA, with its improved spectral resolution over ROSAT, can help elucidate the role of the total emission from discrete sources in NGC 720. However, we must await the launch of AXAF to have the combined spatial and spectral resolution to distinguish models of the origin of the position-angle twist and flattening of the radial profile of the HRI data.

We thank J. Dubinski, A. Fabian, L. Hernquist, W. Mathews, P. Sackett, P. Schechter, D. Syer, J. Tonry, S. Tremaine, and S. Zepf for insightful discussions. This research was supported

by grants NASGW-2681 (through subcontract SVSV2-62002 from the Smithsonian Astrophysical Observatory), and NAG5-2921.

Table 1: X-ray Ellipticities and Position Angles

a (arcsec)	ϵ_M	68%	90%	θ_M	68%	90%	Counts
10.....	0.36	0.06 - 0.37	0.02 - 0.51	75	45 - 132	19 - 160	158
20.....	0.14	0.08 - 0.28	0.03 - 0.36	119	84 - 144	60 - 159	418
30.....	0.39	0.22 - 0.39	0.16 - 0.44	129	131 - 156	123 - 165	527
40.....	0.35	0.25 - 0.40	0.20 - 0.45	155	145 - 162	139 - 167	720
50.....	0.28	0.25 - 0.37	0.20 - 0.41	151	144 - 157	139 - 162	908
60.....	0.35	0.23 - 0.38	0.17 - 0.40	144	139 - 153	133 - 158	977
70.....	0.30	0.24 - 0.38	0.18 - 0.44	134	126 - 144	120 - 149	1130
80.....	0.33	0.25 - 0.39	0.20 - 0.42	124	114 - 130	110 - 135	1220
90.....	0.28	0.23 - 0.36	0.18 - 0.41	118	108 - 125	102 - 130	1351
100.....	0.28	0.17 - 0.34	0.12 - 0.38	112	103 - 123	95 - 129	1427
110.....	0.24	0.19 - 0.35	0.12 - 0.39	110	99 - 124	87 - 131	1537
120.....	0.28	0.18 - 0.35	0.09 - 0.40	111	97 - 121	89 - 130	1611

Note. — The values of ϵ_M (and confidence limits) are computed within an aperture of semi-major axis a on the image having $2.5''$ pixels with the background included; the counts, however, have the background subtracted.

Table 2: Symmetry of X-ray Surface Brightness

Quadrant	$PA = 142^\circ$ ($r = 60''$)	$PA = 114^\circ$ ($60'' \leq r \leq 90''$)
I	303 ± 23	86 ± 18
II	253 ± 21	96 ± 18
III	287 ± 22	82 ± 18
IV	284 ± 22	99 ± 18

Note. — Background-subtracted counts and their associated 1σ uncertainties assuming Poisson statistics. See §3 for an explanation of the regions.

Table 3: Radial Profile Models

Model	R_c (arcsec)	β	Σ_{ds}/Σ_{hg}	χ^2	dof
β - HRI	6 ± 3	0.40 ± 0.03	...	18	7
β - PSPC	18 ± 4	0.49 ± 0.02	...	19	10
β - BOTH	13 ± 3	0.46 ± 0.02	...	53	19
β + DISCRETE	30_{-8}^{+16}	$0.50_{-0.01}^{+0.05}$	$0.40_{-0.20}^{+0.27}$	29	18
SMD - BOTH	46	19
SMD + DISCRETE	$0.40_{-0.27}^{+0.20}$	29	18

Note. — Under “Models”, β stands for the hot gas represented by the β model while SMD indicates the spheroidal mass models found by BC to be consistent with the PSPC data for NGC 720. “BOTH” indicates model is fit jointly to HRI and PSPC data. The DISCRETE models are fit jointly to both data sets. For the SMD models we only list the value of χ^2 and the flux ratio for the DISCRETE case.

REFERENCES

- Aschenbach, B. 1988, *Appl. Opt.*, 27, No. 8, 1404
- Birkinshaw, M., & Davies, R. L. 1985, *AJ*, 291, 32
- Buote, D. A., & Canizares, C. R. 1994, *ApJ*, 427, 86 (BC)
- Buote, D. A., & Canizares, C. R. 1996, *ApJ*, in press (astro-ph/9508005)
- Buote, D. A., & Tsai, J. C. 1995, *ApJ*, 439, 29
- Buote, D. A., & Tsai, J. C. 1996, *ApJ*, in press (astro-ph/9504046)
- Canizares, C. R., Fabbiano, G., & Trinchieri, G. 1987, *ApJ*, 312, 503
- Cavaliere, A., & Fusco-Femiano, R. 1976, *A&A*, 49, 137
- Cowie, L. L., Fabian, A. C., & Nulsen, P. E. J. 1980, 191, 399
- David, L. P., Harnden, F. R., Kearns, K. E., & Zombeck, M. V. 1995, The ROSAT High Resolution Imager (HRI), (U.S. ROSAT Science Data Center – Smithsonian Astrophysical Observatory)
- de Zeeuw, T., in 36th Herstmonceaux Conf., Gravitational Dynamics, ed. O. Lahav, E. Terlevich, & R. Terlevich (Cambridge: Cambridge Univ. Press), in press (astro-ph/9510145)
- de Zeeuw, T., & Franx, M. 1991, *ARA&A*, 29, 239
- Dressler, A., Schechter, P. L., & Rose, J. A. 1986, *AJ*, 91, 1058
- Dubinski, J. 1994, *ApJ*, 431, 617
- Dubinski, J., & Carlberg, R. 1991, *ApJ*, 378, 496
- Dubinski, J., & Kuijken, K. 1995, *ApJ*, 442, 492
- Fabian, A. C. 1994, *ARA&A*, 32, 277
- Forman, W., Jones, C., & Tucker, W. 1985, *ApJ*, 293, 102
- Frenk, C. S., White, S. D. M., Davis, M., Efstathiou, G. 1988, *ApJ*, 327, 507
- Fried, J. W., & Illingworth, G. D. 1994, *AJ*, 107, 992
- Hasinger, G., Burg, R., Giacconi, R., Hartner, G., Schmidt, M., Trümper, J., & Zamorani, G. 1993, *A&A*, 275, 1
- Hernquist, L. 1990, *ApJ*, 356, 359
- Katz, N., & Gunn, J. E. 1991, *ApJ*, 377, 365
- Katz, N., & White, S. D. M. 1993, *ApJ*, 412, 455
- Kim, D.-W., Fabbiano, G., & Trinchieri, G. 1992, *ApJS*, 80, 645
- Kley, W., & Mathews, W. G. 1995, *ApJ*, 438, 100
- Matsushita, K., et. al. 1994, *ApJ*, 436, L41

- Mihalas, D., & Binney, J. 1981, Galactic Astronomy (New York: Freeman)
- Morse, J. A. 1993, in The Soft X-ray Cosmos (AIP Conf. Series 313), ed. E. M. Schlegel, & R. Petre (AIP Press: New York), 252
- Ostriker, E. C., & Binney, J. J. 1989, MNRAS, 237, 785
- Peletier, R. F., Davies, R. L., Illingworth, G. D., Davis, L. E., Cawson, M. 1990, AJ, 100, 1091
- Raymond, J. C., & Smith, B. W. 1977, ApJS, 35, 419
- Sackett, P. D., Gravitational Lensing (IAU Symp. 173), ed. C. S. Kochanek, & J. N. Hewitt (Dordrecht: Reidel), in press (astro-ph/9508098)
- Schechter, P. L. 1987, in Structure and Dynamics of Elliptical Galaxies (IAU Symp. 127), ed. T. de Zeeuw (Dordrecht: Reidel), 217
- Stark, A. A., et al. 1992, ApJS, 79, 77
- Statler, T. S. 1994a, ApJ, 425, 458
- Statler, T. S. 1994b, AJ, 108, 111
- Trinchieri, G., Fabbiano, G., & Canizares, C., 1986, ApJ, 310, 637
- Trümper, J. 1983, Adv. Space Res., 2, 241

Fig. 1.—

Contour map of the HRI X-ray surface brightness of the E4 galaxy NGC 720 binned into $5''$ pixels for display; the contours are separated by a factor of 2 in intensity and the direction of Celestial North is up and East to the left. The image has been corrected for the effects of exposure variations and telescopic vignetting. The image has been smoothed for visual clarity with a Gaussian of $\sigma = 1$ pixel, although the image used for analysis is not smoothed as such.

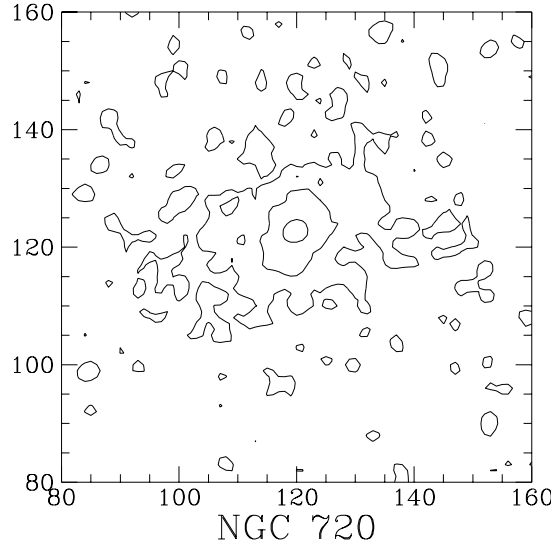


Fig. 2.—

The HRI position angle computed within a specified semi-major axis, a , and the estimated 95% confidence intervals; note the position angles are correlated since each a contains the regions $< a$. The optical and PSPC PA are shown approximately over their relevant range of validity.

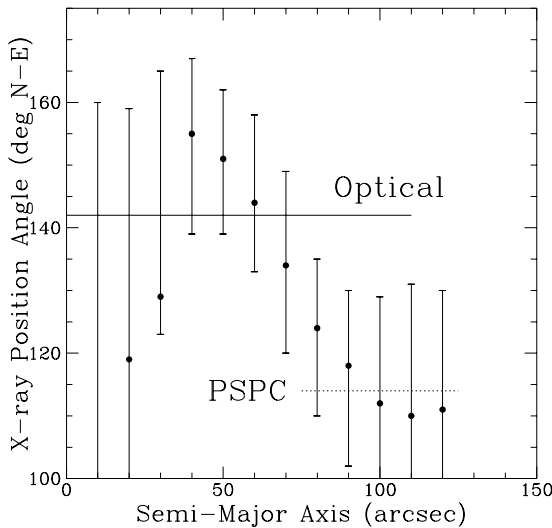


Fig. 3.—

(a) The HRI background-subtracted radial profile binned such that each bin has $S/N \geq 6$. The solid line represents the best-fit β model and the dotted line corresponds to the best-fit $\beta +$ discrete model. The midpoint of each bin is used to define its location in the plot; note the lines are only defined at the midpoints of the bins. The dashed horizontal lines represent the background levels. (b) The PSPC background-subtracted radial profile binned such that each bin has $S/N > 5$. The squares and crosses represent the corresponding best-fit models from (a).

